Advanced coded-aperture imaging system for nuclear medicine

Nagaaki Ohyama, Toshio Honda, Jumpei Tsujiuchi, Toru Matumoto,
Takeshi A. Iinuma, and Kenji Ishimatsu

An advanced coded imaging system is described, and some results of phantom experiments are presented. The advanced method uses a pair of coherent codes (+1 and −1 codes) and has many advantages compared with conventional ones. One of the greatest advantages is that there are no sidelobes in the focal plane and only a few in other planes. Therefore, when an object can be regarded as two-dimensional, it is perfectly reconstructed with high detecting efficiency, and this is successfully simulated by a thyroid phantom with ^{99m}Tc. Moreover, this system has an ability to reconstruct tomograms, which is also shown by using ring phantoms piled on one another with some cold spots in their shells. From these experimental results it may be concluded that the new system is useful for practical applications, for example, to nuclear medicine.

I. Introduction

In γ-ray imaging systems for medical diagnosis it has been very desirable to realize higher detection efficiency so as to improve the quality of reconstructed images. For this purpose, use of a large coded aperture is fairly promising, because it uses in general a specially designed aperture with high sensitivity instead of conventional ones. Many studies of various kinds of aperture and decoding method have been reported so far, for example, Fresnel zone plates[1] and stochastic,[2] random pinhole,[3] and Fourier apertures.[4] Possibilities for practical use are shown by them, but they are not so satisfactory. When such apertures are used for coding, some postprocessing will be necessary to reconstruct an image of an object.

Generally, multipinhole systems use a correlation method in the decoding step, that is, a sort of digital matched filtering. By this method, however, there should be many sidelobes blurring reconstructed images, which are due to much overlap of the projected images through pinholes. To diminish the total number of sidelobes, for example, the mismatched method[5] and coherent codes method[6] were proposed. Both methods use +1 and −1 codes, but they cannot clear away all the sidelobes. Consequently, it is true that detection efficiency can be improved, but the SNR of reconstructed images cannot be increased because of the ghosts caused by the insuppressible sidelobes.

The authors have proposed an advanced coded imaging method[7,8] which can clear away all the sidelobes by using a pair of coherent codes when an object can be regarded as a 2-D one. In the case of 3-D objects, however, it is still impossible to clear them away even by this method or by any other conventional method except for the time-modulated aperture method. But the time-modulated aperture method dealt with in Ref. 9 is not favorable in terms of noise behavior; i.e., separation of the overlapped images will greatly increase the statistical deviations. Furthermore, the method needs a number of recording times greater than or equal to the number of pinholes used in the system. Too many recording times would cause much time loss during the aperture change and require a large computer memory. But, in a special case, when some projected images are spatially separated from one another by themselves, we can reduce the necessary recording times properly as shown in Ref. 8. The advanced coding method needs only four recording times no matter how many pinholes are used. The abilities of this method to reconstruct tomograms are clearly shown and discussed in detail in the previous paper.[10]

This paper shows the advanced coded imaging system and successful results of phantom experiments. As a 2-D object, a thyroid phantom filled with ^{99m}Tc is projected onto a gamma camera through sixteen pinholes with four kinds of coding plate, which realize a pair

Kenji Ishimatsu is with Hitachi Medical Corporation, Kashiwa Works, 2-1 Shintoyohuta, Kashiwa 277, Japan; T. Matumoto and T. A. Iinuma are with National Institute of Radiological Sciences, 4-9-1 Anagawa, Chiba 260, Japan; the other authors are with Tokyo Institute of Technology, Imaging Science & Engineering Laboratory, 4259 Nagatsuta, Midoriku, Yokohama 227, Japan.

Received 5 April 1983.
0003-6935/83/223555-07$01.00/0.
© 1983 Optical Society of America.

of coherent codes. To simulate tomographic reconstruction, ring phantoms are also used with some cold spots which are piled on one another to imitate a human myocardium. Good reconstructed images will be shown in the following sections.

II. Basic Principles

In a coded aperture system applied to nuclear medicine, an object is projected onto a gamma camera through a specially designed aperture as schematically shown in Fig. 1. In case of a planar object the recorded image R is given by the convolution of the object O and the aperture arrangement P, and this is expressed in mathematical form as

$$R = O * P, \tag{1}$$

where $*$ denotes a convolution operation. And for a volume object, where we suppose that the object consists of n layers, Eq. (1) can be written by using a set of O_k and P_k as

$$R = \sum_{i=1}^{n} O_i * P_i, \tag{2}$$

where the P_k differs only by a scaling transformation in the coordinates, and n is determined in practice by the object size and depth resolution. In the decoding step an adequate function P'_k is correlated with R giving the reconstructed image of the kth layer O'_k, and this is represented by

$$O'_k = R \star P'_k = \sum_{i=1}^{n} O_i * P_i \star P'_k, \tag{3}$$

where $\star$ denotes the correlation operation. From Eq. (3), it is easily conjectured that the kth layer of the object can be perfectly reconstructed if the following conditions are satisfied:

$$P_k \star P'_k = \delta \tag{4}$$

$$P_k \star P'_m = 0 \qquad (k \neq m), \tag{5}$$

where δ is the delta-function. But neither of these conditions can be satisfied. Therefore, most images reconstructed by conventional coded imaging method always suffer from ghosts due to insuppressible sidelobes.

A. Principle for Planar Objects

The advanced coded method uses a pair of coherent codes, P and G, to satisfy the following condition instead of Eq. (4):

$$P \star P + G \star G = 2N\delta, \tag{6}$$

where N is the number of pinholes that compose the aperture. The basic pair with two pinholes ($N = 2$) are already known:

$$P = -\delta(x - a) + \delta(x + a); \tag{7}$$

$$G = \delta(x - a) + \delta(x + a). \tag{8}$$

Equation (7) indicates that P has a plus pinhole at the location $x = -a$ and a minus one at $x = a$, and also Eq. (8) indicates that G has two plus pinholes at $x = \pm a$.

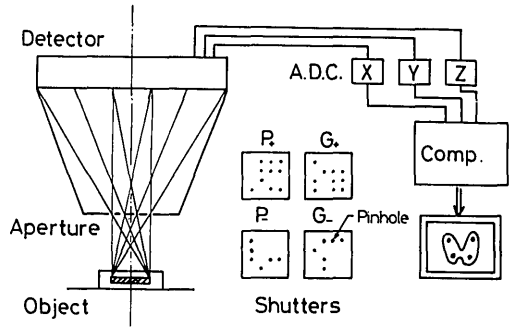

Fig. 1. Schematic diagram of system operation. This system uses four kinds of shutter to realize a pair of coherent codes.

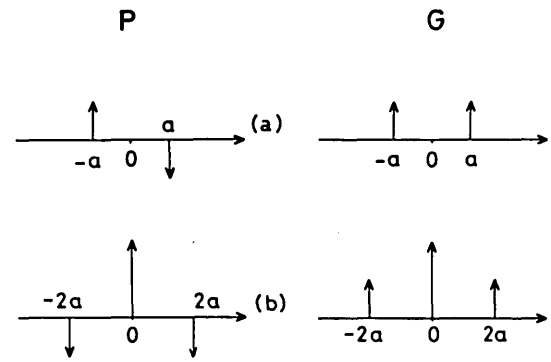

Fig. 2. (a) Basic pair of 2 × 1 codes; (b) their autocorrelations. An upward arrow is a plus pinhole, and a downward one is a minus one

These codes and their autocorrelations are shown in Fig. 2, where we can easily understand that all the sidelobes appearing in both autocorrelations will be canceled by adding them to each other. Namely, the basic pair expressed by Eqs. (7) and (8) surely satisfies the condition required for planar objects to be completely reconstructed without any artifacts.

Once we know a pair which satisfies Eq. (6), we can easily get other pairs with more pinholes in accordance with the following equations:

$$P' = P + G, \tag{9}$$

$$G' = P - G, \tag{10}$$

and this is easily verified; autocorrelations of P and G are given by

$$P' \star P' = P \star P + G \star G + P \star G + G \star P, \tag{11}$$

$$G' \star G' = P \star P + G \star G - P \star G - G \star P. \tag{12}$$

The addition of them becomes

$$P' \star P' + G' \star G' = 2(P \star P + G \star G). \tag{13}$$

As P and G satisfy Eq. (6), Eq. (13) will be reduced to

$$P' \star P' + G' \star G' = 4N\delta. \tag{14}$$

This result means that P' and G' are the pair with $2N$ pinholes derived from the one with N pinholes. Thus

we can get many pairs with a sufficient number of pinholes and realize desirable detection efficiency. Further discussion is presented in detail in Ref. 7.

For example, Fig. 3 shows a pair of 2 × 2 codes derived from the basic pair. Also, Fig. 4(a) shows a pair of 4 × 4 codes used in this experiment and their derivations, and Fig. 4(b) gives their autocorrelations. Notice in Fig. 4(b) that for any sidelobe there must be another whose sign is opposite to the first one. Therefore, they can be cleared away by adding the images. This means that the addition of the autocorrelations of P and G yields a delta-function; that is, it satisfies the condition (6).

B. Principle for Volume Objects

To reconstruct good tomograms of a volume object, the other condition corresponding to Eq. (5) should be satisfied:

$$P_k \star P_m + G_k \star G_m = 0 \qquad (k \neq m). \tag{15}$$

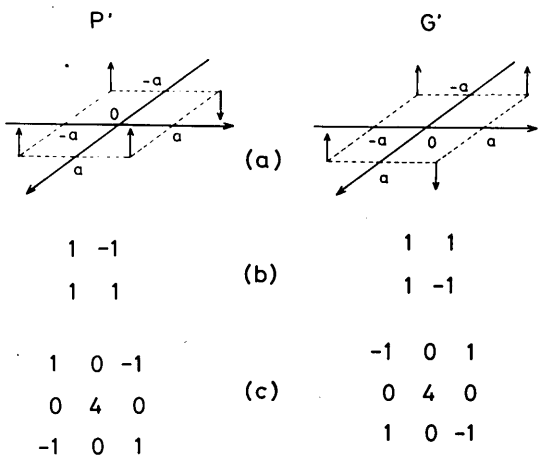

Fig. 3. (a) Pair of 2 × 2 codes; (b) their matrix expressions; (c) their autocorrelations.

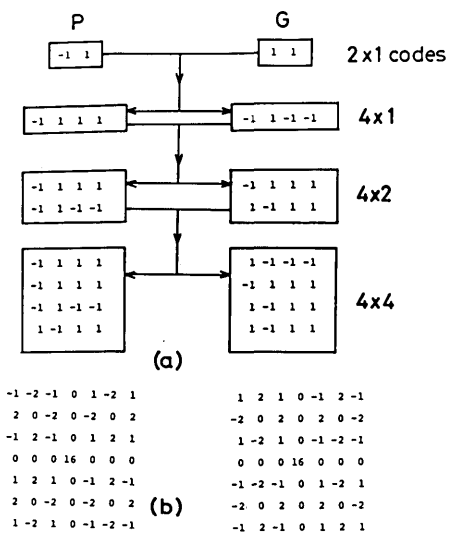

Fig. 4. (a) Pair of 4 × 4 codes used in this experiment and their derivations; (b) their autocorrelations. Notice that sidelobes are completely cleared away by adding them to each other.

However, the advanced coded method, as well as others, fails to satisfy the condition (15). Consequently, reconstructed images of each layer are always degraded by both the defocused images of other layers and the artifacts caused by insuppressible sidelobes.

Then, an iterative method is applied to satisfy condition (15). The basic algorithm and a computer simulation are shown in Ref. 10. Here only a brief explanation is presented; after the two kinds of image, R_1 and R_2, are recorded by a pair of coherent codes, they are, respectively, correlated with the corresponding decoding functions to give initial guesses for each layer:

$$\begin{aligned} O_k^0 &= R_1 \star P_k + R_2 \star G_k \\ &= \sum_{i=1}^{n} O_i * (P_i \star P_k + G_i \star G_k), \end{aligned} \tag{16}$$

where the superscript 0 indicates the initial guess. Substituting Eq. (6) into Eq. (16), we can derive

$$O_k^0 = O_k + \sum_{i=1}^{n} {}'O_i * (P_i \star P_k + G_i \star G_k). \tag{17}$$

The second term on the right-hand side should be as small as possible. Then, we rewrite Eq. (17), denoting the second term as a ghost g:

$$O_k^0 = O_k + g_k^0. \tag{18}$$

According to an actual recording step, $\{O_k^0\}$ are coded by P and G in the computer making the projection images of them, and they are subtracted by the corresponding real records, which gives two coded images of the first ghosts $\{g_k^0\}$:

$$R_1 = \sum_{i=1}^{n} g_i^0 * P_i; \tag{19}$$

$$R_2 = \sum_{i=1}^{n} g_i^0 \star G_i. \tag{20}$$

The same decoding process will be carried out to get a set of ghosts $\{g_k^0\}$:

$$\begin{aligned} C_k^0 &= g_k^0 + \sum_{i=1}^{n} {}'g_i^0 * (P_i \star P_k + G_i \star G_k) \\ &= g_k^0 + g_k^1. \end{aligned} \tag{21}$$

Subtracting C_k^0 from O_k^0, we can have

$$O_k^1 = O_k^0 - C_k^0 = O_k - g_k^1. \tag{22}$$

If g_k^1 is less than g_k^0, O_k^∞ becomes equal to O_k after sufficient repetitions. Thus, it will be possible to reconstruct tomograms by the advanced coded method with iterative processing.

III. Experimental Results

A specially designed aperture, as shown in Fig. 5, has been made for this system. It consists of 4 × 4 pinholes arranged like a square grid with four kinds of coding plate to realize a pair of coherent codes. All the pinhole diameters are 3 mm, and they are placed at 15-mm intervals. The aperture is equipped with a large-field gamma camera, Hitachi RC1C-1635DL, controlled by an EDR4200 system, and four recording times are implemented, changing the coding plates sequentially.

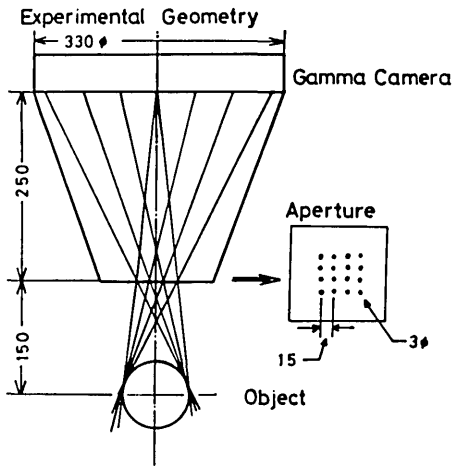

Fig. 5. Multipinhole collimator and aperture. This aperture has sixteen pinholes of 3-mm diam arranged like a square grid at 15-mm intervals. On this aperture is set a shutter plate to close some pinholes according to the codes.

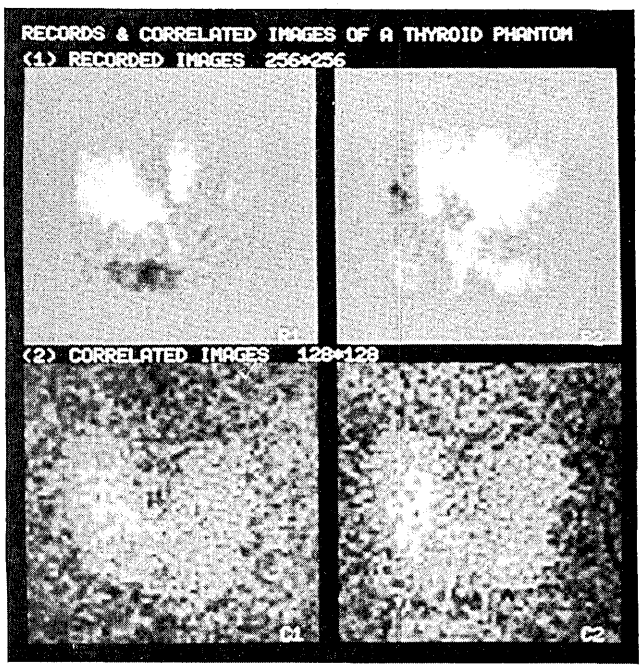

Fig. 6. (a) Pair of recorded images of a thyroid phantom with ^{99m}Tc. (b) Correlated images by corresponding codes, P and G. There still remains a strong ghost caused by the insuppressible sidelobes.

Detected events are reduced to the X, Y position and Z-energy signals, and they are sent to a minicomputer, a Hitac10-II, to form digital projection images. Then, the other minicomputer, an Eclipse S-130, implements the reconstruction procedures to display the images of the object on a color CRT.

A. Thyroid Phantom Experiment (2-D Object)

A thyroid phantom with 15-mm thickness is used as a planar object filled with ^{99m}Tc. The distance between the aperture and the object surface is ~15 cm, and that between the aperture and the detector, NaI(T1) crystal, is 25 cm. Thus the magnification becomes ~1.67. As the size of the phantom is 6 × 7 cm^2, one image on the detector projected through a pinhole becomes ~10 × 12 cm^2. Due to the collimator size and pinhole arrangement, the interval between two adjacent image centers will be 4 cm when the object is placed 15 cm from the aperture. Then, it is expected that there should be considerable overlap between projected images.

Figure 6(1) shows the two kinds of recorded image, each with 256 × 256 elements, with much overlap, which are, respectively, obtained by the subtraction of one image, recorded by the negative pinholes composed of P or G, from the other image, composed of the corresponding positive ones. In the decoding step, these recorded images are, respectively, correlated with P or G, resulting in Fig. 6(2), and these images, 128 × 128 pixels, including many ghosts, are the very ones obtainable by the coherent code method. Then, they are added to give a reconstructed image of high quality without sidelobes. In this experiment, image reconstruction is accomplished under four types of condition: with or without a lewisite scattering plate of 6-cm thickness and with or without energy gating of the photopeak. These four conditions are used to simulate the scattering phenomena in a human body and to estimate how much they degrade the reconstructed images. These reconstructed images are shown in Fig. 7, while Fig. 8 shows the single-pinhole images recorded in the same condition and experimental geometry. The recording time for single-pinhole images is also 4 min, which is the same as the total time of the multipinhole images. Comparing Fig. 7 with Fig. 8, we can see that multipinhole images have higher quality or less amount of noise than single-pinhole ones in any case. To appreciate this, we will calculate the deviations and SNR of these images within two areas as shown in Fig. 9. The results are summarized in Table I, which again assures us of the ability of this method to reconstruct good images.

B. Ring Phantom Experiment (3-D Object)

To simulate tomographic reconstruction, a sheet of filter paper was cut into a ring similar to a sliced image of human myocardium. Three kinds of ring containing ^{99m}Tc are piled on one another in the order shown in Fig. 10, and they are also illustrated, for the purpose of easier appreciation, in the same size as projected on the detector.

Figure 11 shows the obtained records coded by P and G after four recording times. The image size is 128 × 128, and the total count of detected events is ~4,890,000 with a 10% energy window. When the energy of a detected γ ray is within a certain width of the photopeak, in this case 140 ± 7 keV, it will contribute to the records, but otherwise it will be rejected. Thus we can reduce the undesirable influence of Compton scattering.

Figure 12 shows the initial guesses of seven layers, 64 × 64 pixels, obtained by the procedure of Eq. (16), where in P_k and P_{k+1} as well as in G_k and G_{k+1} the parallax difference between the adjacent pinholes and layers is only 1 pixel. Due to the collimator size and the experimental geometry shown in Fig. 10, tomograms are reconstructed at 97, 105, 114, 127, 137, 153, 173 mm

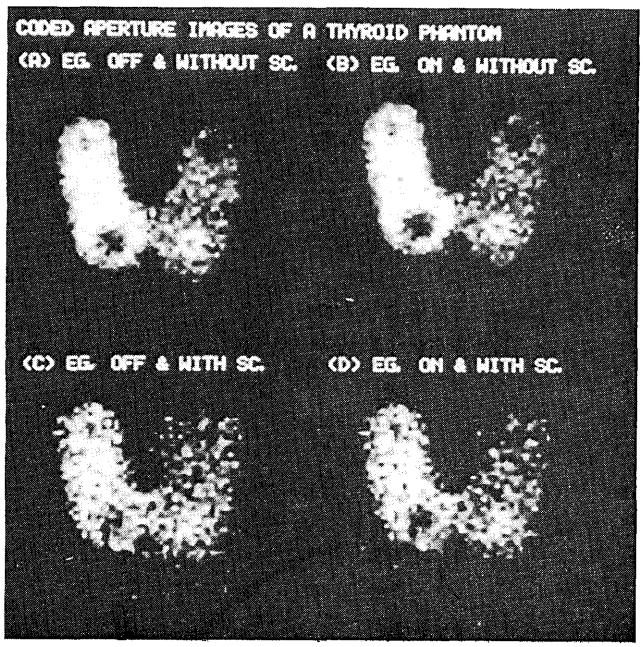

Fig. 7. Multipinhole images of the thyroid phantom reconstructed in different conditions: (a) energy gate off, without scatter plate; (b) energy gate on, without scatter plate; (c) energy gate off, with scatter plate; (d) energy gate on, with scatter plate. Total counts of the contributed events to reconstruction are, respectively, (a) 349,171, (b) 274,296, (c) 206,148, (d) 127,676.

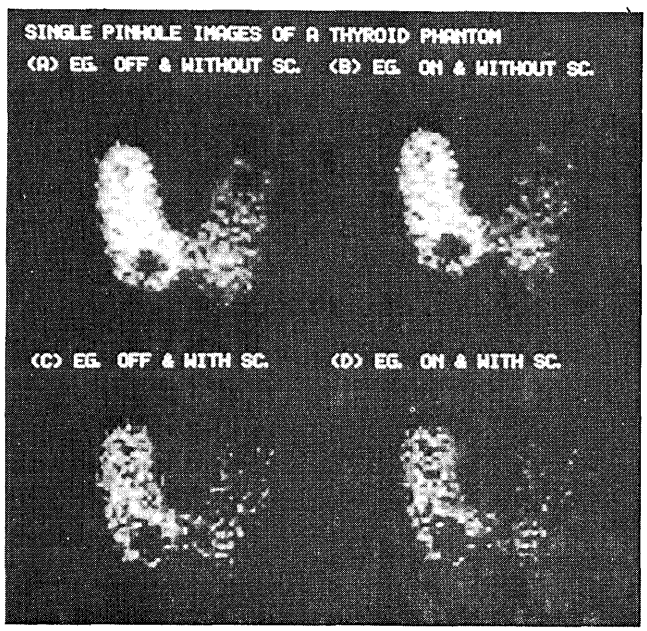

Fig. 8. Single-pinhole images recorded under the same conditions as shown in Fig. 7: (a) energy gate off, without scatter plate; (b) energy gate on, without scatter plate; (c) energy gate off, with scatter plate; (d) energy gate on, with scatter plate. Total counts of each image are, respectively, (a) 60,000, (b) 40,643, (c) 29,560, (d) 17,920.

away from the aperture, and phantoms are located at 105, 125, 155 mm. Thus in Fig. 12 $LY = 2, LY = 4, LY = 6$ are the focused images. Since these initial guesses are so degraded by both ghosts caused by insuppressible sidelobes and by overlapping of defocused images of other layers, we cannot recognize the real shape of interest.

Figure 13 shows the reconstructed images of seven layers obtained after five cycles of iteration. This procedure needs ~8 min with FORTRAN V in the Eclipse S-130 minicomputer. Comparing Fig. 13 with Fig. 12, we can see that the image quality is considerably improved enough to recognize the shapes of the phantoms, mainly the region of interest, without failure. But, as is true for such systems that are to reconstruct longi-

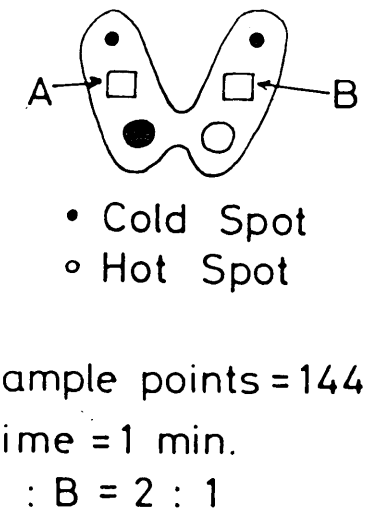

Fig. 9. Sampled areas for evaluating the deviations and SNRs.

Table I. Signal-to-Noise Ratios of Obtained Images by Multipinhole and Single-pinhole Collimator

Energy gate	Area	Collimator	Average	Deviation	SNR (avg./dev.)	SNR up (%)
(1) Without scatterer						
Off	*A*	M	112.9	17.9	6.3	21
		S	19.2	3.2	5.2	
	B	M	61.5	19.4	3.2	11
		S	10.2	3.6	2.9	
On	*A*	M	97.3	17.4	5.6	26
		S	15.1	3.4	4.4	
	B	M	52.1	16.7	3.1	11
		S	7.3	2.6	2.8	
(2) With scatterer						
Off	*A*	M	51.5	14.3	3.6	29
		S	7.3	2.6	2.8	
	B	M	29.9	11.9	2.5	12
		S	4.2	2.1	2.2	
On	*A*	M	39.5	11.8	3.3	39
		S	5.3	2.2	2.4	
	B	M	22.2	10.1	2.2	35
		S	2.9	1.8	1.6	

tudinal tomograms, the depth resolution normal to the aperture is in general not so good. Then, a cold spot in a layer tends to have some influence on the other layers, especially the adjacent one. This is seen in Fig. 13; $LY = 2$ has a strong cold spot in the upper right of the shell. Thus it casts its shadow on the other plane as seen, for example, in $LY = 4$. Consequently, it may be dangerous by examining only one image, not all images, to judge whether there is any defect (cold spot) in the layer. Further developments of reconstructing algorithm should be necessary to improve the depth resolution to obtain better tomograms.

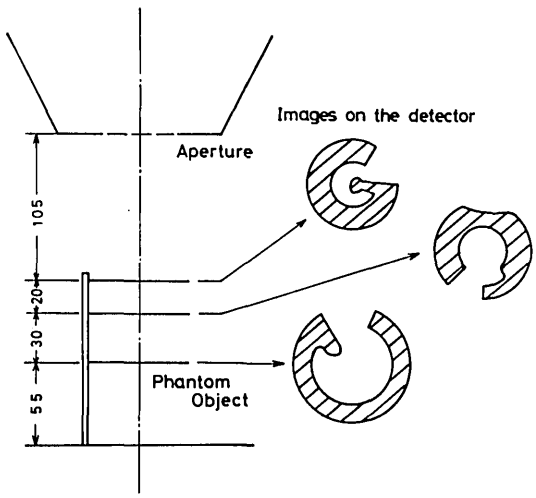

Fig. 10. Experimental geometry for tomogram reconstruction and shapes of ring phantoms on the detector.

IV. Summary and Conclusion

This paper shows an advanced coded imaging system that uses a pair of coherent codes and some successful results of phantom experiments of planar and volume objects. In both cases, reconstructed images are fairly good in quality, which is mainly due to the following two advantages: one is the higher detection efficiency. Since this system uses a sixteen-pinhole aperture and needs only four recording times, the detection efficiency is increased about eight times compared with a single-pinhole system. The other advantage is the size of each projected image through a pinhole. Since the advanced coded method permits considerable overlap in the records, one image projected through a pinhole can be enlarged to improve the spatial resolution within the limited camera size.

The design of a collimator should be changed according to the purpose. Namely, a collimator for planar objects should have an aperture in which pinholes are arranged closely, so as not to produce much parallax, while one for a tomographic system needs an aperture to the contrary. From this point of view, the depth resolution of this system as shown in this paper can be improved, because the collimator was designed just for planar objects with closely arranged pinholes.

These good experimental results ensure that this system will have practical application in nuclear medicine.

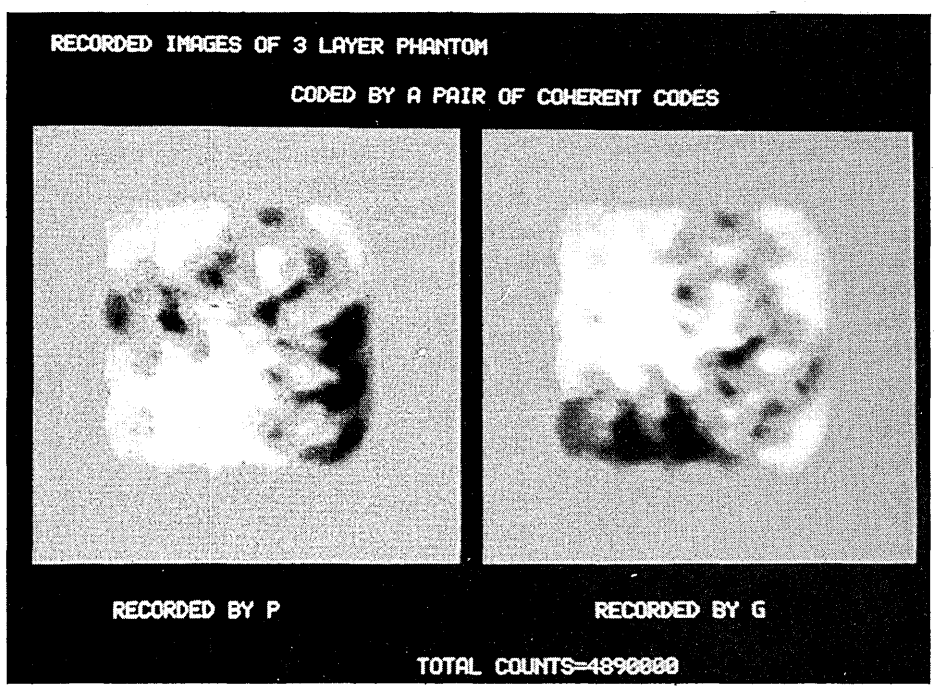

Fig. 11. Obtained records of the ring phantoms coded by P and G. Total recording time is 200 sec, and detected events are ~4,890,000.

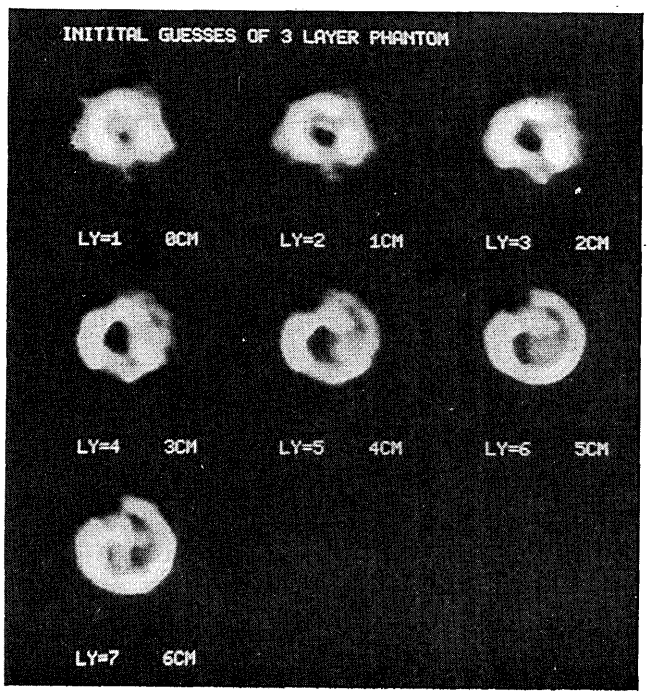

Fig. 12. Initial guesses of seven-layer reconstruction. These images are not good enough to recognize the regions of interest.

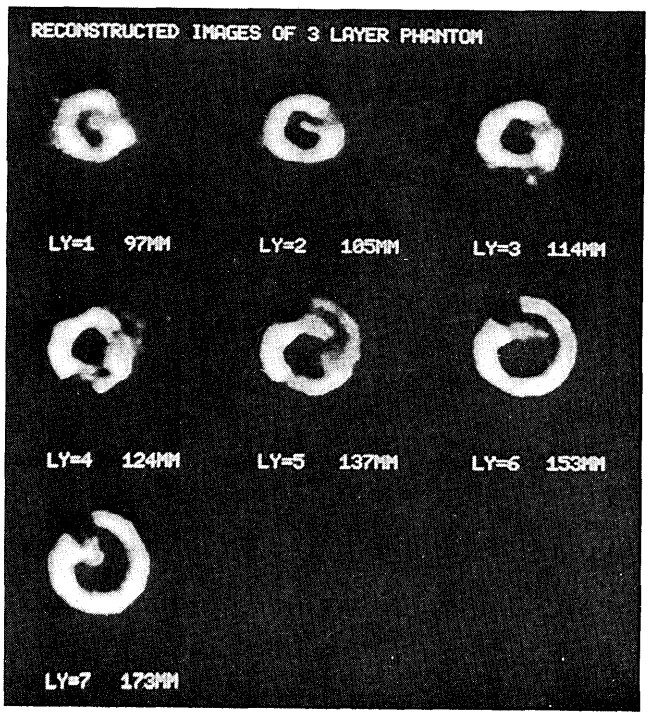

Fig. 13. Reconstructed images after five iterations. Images become much better than the initials, so we can easily find the defects (cold spots) of ring phantoms.

References

1. H. H. Barrett and F. A. Horrigan, Àppl. Opt. **12,** 2686 (1973).
2. R. S. May, Z. Akcasu, and G. F. Knoll, Appl. Opt. **13,** 2589 (1974).
3. G. W. Stroke, G. S. Hayat, R. B. Hoover, and J. H. Underwood, Opt. Commun. **1,** 138 (1969).
4. C. Chou and H. H. Barrett, Opt. Lett. **3,** 187 (1978).
5. C. Brown, J. Appl. Phys. **45,** 1806 (1974).
6. H. Weiss, E. Klotz, R. Linde, G. Rabe, and U. Tiemens, Opt. Acta **24,** 305 (1977).
7. N. Ohyama, T. Honda, and J. Tsujiuchi, Opt. Commun. **27,** 339 (1978).
8. N. Ohyama, "New Coded Aperture Methods for Reconstructing Tomograms and Applications to Nuclear Medicine," Ph.D. Thesis, Imaging Science and Engineering Laboratory, Tokyo Institute of Technology (1982), p. 51.
9. D. Rosenfeld and A. Macovski, IEEE Trans. Nucl. Sci. **NS-24,** 570 (1977).
10. N. Ohyama, T. Honda, and J. Tsujiuchi, Opt. Commun. **36,** 434 (1981).